



Kristina M. Mueller,^{1,2} Kerstin Hartmann,³ Doris Kaltenecker,² Sabine Vettorazzi,³ Mandy Bauer,³ Lea Mauser,³ Sabine Amann,⁴ Sigrid Jall,^{5,6} Katrin Fischer,^{5,6} Harald Esterbauer,⁴ Timo D. Müller,^{5,6} Matthias H. Tschöp,^{5,6} Christoph Magnes,⁷ Johannes Haybaeck,⁸ Thomas Scherer,⁹ Natalie Bordag,¹⁰ Jan P. Tuckermann,³ and Richard Morigg^{1,2,11}

Adipocyte Glucocorticoid Receptor Deficiency Attenuates Aging- and HFD-Induced Obesity and Impairs the Feeding-Fasting Transition



Diabetes 2017;66:272–286 | DOI: 10.2337/db16-0381

Glucocorticoids (GCs) are important regulators of systemic energy metabolism, and aberrant GC action is linked to metabolic dysfunctions. Yet, the extent to which normal and pathophysiological energy metabolism depend on the GC receptor (GR) in adipocytes remains unclear. Here, we demonstrate that adipocyte GR deficiency in mice significantly impacts systemic metabolism in different energetic states. Plasma metabolomics and biochemical analyses revealed a marked global effect of GR deficiency on systemic metabolite abundance and, thus, substrate partitioning in fed and fasted states. This correlated with a decreased lipolytic capacity of GR-deficient adipocytes under postabsorptive and fasting conditions, resulting from impaired signal transduction from β -adrenergic receptors to adenylate cyclase. Upon prolonged fasting, the impaired lipolytic response resulted in abnormal substrate utilization and lean mass wasting. Conversely, GR deficiency attenuated aging-/diet-associated obesity, adipocyte hypertrophy, and liver steatosis. Systemic glucose tolerance was improved in obese GR-deficient mice,

which was associated with increased insulin signaling in muscle and adipose tissue. We conclude that the GR in adipocytes exerts central but diverging roles in the regulation of metabolic homeostasis depending on the energetic state. The adipocyte GR is indispensable for the feeding-fasting transition but also promotes adiposity and associated metabolic disorders in fat-fed and aged mice.

Energy homeostasis requires the integration of multiple signals between the central nervous system and the periphery to adjust substrate distribution in accordance with metabolic demands. The steroid hormones glucocorticoids (GCs) are important integrators in the body's adaptation to energetic stress by regulating several components of energy homeostasis, including glucose and lipid metabolism (1,2). Consequently, states of chronic GC exposure are associated with metabolic dysfunctions (1,2). The cellular effects of GCs are mediated in large part through

¹Institute of Animal Breeding and Genetics, University of Veterinary Medicine Vienna, Vienna, Austria

²Ludwig Boltzmann Institute for Cancer Research, Vienna, Austria

³Institute for Comparative Molecular Endocrinology, University of Ulm, Ulm, Germany

⁴Department of Laboratory Medicine, Medical University of Vienna, Vienna, Austria

⁵Institute for Diabetes and Obesity, Helmholtz Diabetes Center, Helmholtz Zentrum München, German Research Center for Environmental Health (GmbH) and German Center for Diabetes Research (DZD), Neuherberg, Germany

⁶Division of Metabolic Diseases, Department of Medicine, Technische Universität München, Munich, Germany

⁷HEALTH Institute for Biomedicine and Health Sciences, JOANNEUM RESEARCH, Forschungsgesellschaft mbH, Graz, Austria

⁸Institute of Pathology, Medical University of Graz, Graz, Austria

⁹Division of Endocrinology and Metabolism, Department of Medicine III, Medical University of Vienna, Vienna, Austria

¹⁰Center for Biomarker Research in Medicine, CBmed GmbH, Graz, Austria

¹¹Medical University of Vienna, Vienna, Austria

Corresponding authors: Richard Morigg, richard.morigg@lbicr.lbg.ac.at, and Jan P. Tuckermann, jan.tuckermann@uni-ulm.de.

Received 24 March 2016 and accepted 14 September 2016.

This article contains Supplementary Data online at <http://diabetes.diabetesjournals.org/lookup/suppl/doi:10.2337/db16-0381/-/DC1>.

K.M.M. and K.H. contributed equally to this work, and J.P.T. and R.M. contributed equally to this work.

© 2017 by the American Diabetes Association. Readers may use this article as long as the work is properly cited, the use is educational and not for profit, and the work is not altered. More information is available at <http://www.diabetesjournals.org/content/license>.

activation of the glucocorticoid receptor (GR). The understanding of how tissue-specific functions of the GC-GR axis contribute to systemic energy metabolism has been substantially extended by mouse models of discrete GR deficiency in liver and muscle (1,3,4).

The most abundant energy reservoir in mammals is white adipose tissue (WAT), which allows nonadipose tissues to function normally under conditions of overnutrition or fasting (5,6). Thus, an appropriate control in WAT to store and release energy in response to changes in nutrient availability is critical for metabolic homeostasis. GCs were shown to induce lipolysis (7–9), to stimulate lipogenesis in the presence of insulin (10,11), and to promote lipid storage, uptake, and mobilization (2,9,12). An increase of local GC regeneration by the enzyme 11 β -hydroxysteroid dehydrogenase 1 (11 β -HSD1) within WAT suggests a role of the adipocyte GC-GR axis in common obesity (2,12–16). These lines of evidence are consistent with a central role of GCs in regulating energy metabolism. However, the exact physiological importance of the adipocyte GR for the maintenance of systemic metabolic homeostasis is yet to be determined.

To delineate this undefined role of the GR, we used an adipocyte-specific gene knockout strategy in mice. We demonstrate that adipocyte GR significantly impacts systemic nutrient partitioning in different energetic states. While GR deficiency disrupts the feeding-fasting transition, it ameliorates obesity and its associated metabolic disorders, thus exerting opposing roles in the regulation of metabolic homeostasis.

RESEARCH DESIGN AND METHODS

Animal Experiments

Adipocyte-specific GR-deficient mice (Nr3c1^{tm2Gsc}Tg(Adipoq-cre)1Evd; GR ^{Δ Adip}; C57BL/6 x FVB/N) were generated by crossing *Nr3c1 floxed* (17) with *Adipoq-cre* mice (18). *Adipoq-cre* negative littermates served as controls (Nr3c1^{tm2Gsc}). Animals were housed under standardized conditions (12-h dark/12-h light cycle) and fed a regular diet (Ssniff EF, R/M Kontrolle; Ssniff GmbH, Soest, Germany). For high-fat diet (HFD) experiments, mice received either Ssniff EF acc.D12492 (34.6% crude fat) or Ssniff EF D12450B mod. Animal studies were approved by the Austrian government and the Medical University of Vienna (BMWF-66.009/0132-II/3b/2013) and by the Regional Commission Tuebingen, Germany (TVA1126). Except for HFD and aging experiments, 8-week-old male mice were used.

Body composition was determined using EchoMRI-100H (EchoMRI LLC, Houston, TX). μ -CT was performed with in vivo X-ray microtomograph Skyscan 1176 (RJL Micro & Analytic GmbH, Karlsdorf-Neuthard, Germany). Fat volume was reconstructed and calculated using NRecon (version 1.6.9.18) and CTAAn (version 1.14.4.1+).

Glucose and pyruvate tolerance tests (GTTs and PTTs) were performed in 12–16 h-fasted mice; insulin tolerance tests (ITTs) were performed in 4 h-fasted mice. Glucose (2 g/kg) was administered orally or by intraperitoneal

injection (HFD experiments); pyruvate (2 g/kg) and insulin (0.75 units/kg) were given intraperitoneally. Blood glucose levels were determined from the tail vein using a glucometer.

Cold tolerance was determined in 4 h-fasted animals. Mice were housed separately with free access to water at 4°C. Rectal temperature was measured at indicated time points using a BIO-TK9882 thermometer (Bioseb, Vitrolles, France).

Energy expenditure (EE), locomotor activity, respiratory exchange ratio (RER), and food intake were measured by combined indirect calorimetry over 93.4 h (PhenoMaster; TSE Systems, Bad Homburg vor der Höhe, Germany) as described previously (19).

Metabolite and Hormone Measurements

β -Ketones were measured from tail vein blood (Freestyle Precision Xceed, Abbott, Alameda, CA). Nonesterified fatty acids (NEFAs) were determined with the NEFA-HR (2) kit (Wako Chemicals, Neuss, Germany), glycerol with the Free Glycerol Reagent (Sigma-Aldrich, St. Louis, MO), and triglycerides (TGs) and cholesterol were measured with a Reflotron Plus analyzer (Roche, Basel, Switzerland). Insulin, corticosterone, and FGF21 were determined by ELISA (Ultra-Sensitive Mouse Insulin ELISA [Crystal Chem, Downers Grove, IL], Corticosterone ELISA [Enzo Life Sciences, Farmingdale, NY], and Mouse/Rat FGF-21 Quantikine-ELISA [R&D Systems, Minneapolis, MN]). Liver TG content was determined using a Triglyceride Colorimetric Assay (Cayman Chemical, Ann Arbor, MI).

Lipolysis Assays

Epididymal WAT (eWAT) was surgically removed and lipolysis was measured as previously described (20). Stimulations were performed with insulin (30 ng/mL), isoproterenol, forskolin, formoterol, or CL-316,243 (all 10 μ mol/L) for 120 min. NEFA was determined as previously described, and cAMP content in WAT explants by the cAMP complete ELISA (Enzo Life Sciences). Measurements were normalized to tissue weights.

Histology

Tissues were fixed in 4% buffered formalin, paraffin embedded, sectioned, and stained with hematoxylin-eosin (H-E) using standard procedures. Adipocyte sizes were quantified from at least three to five different fields per mouse and at least 20–60 cells/field using ImageJ (Rasband, W.S., ImageJ; NIH, Bethesda, MD, <https://imagej.nih.gov/ij/>). Histological evaluation of livers was performed by a board-certified pathologist (J.H.).

Molecular Analyses

RNA was extracted using commercial kits (Qiagen, Hilden, Germany; Peqlab, Erlangen, Germany). RNA (1 μ g) was reverse transcribed using cDNA synthesis kits (Thermo Fisher Scientific, Waltham, MA; Applied Biosystems, Foster City, CA). Quantitative real-time PCR (qRT-PCR) was performed on an Eppendorf Realplex system using the Taq DNA Polymerase Kit (Eppendorf, Hamburg, Germany) or

on a ViiA7RT-PCR System using the Platinum Sybr Green qPCR Supermix-UDG (Life Technologies, Carlsbad, CA). Gene expression was normalized to *Gapdh* or *Actb* (β -actin) mRNA. Primer sequences are provided in Supplementary Table 1.

Western blot analyses (40 μ g protein) were performed as previously described (21). Primary antibodies against HSC70 (sc-7298), GR (sc-1004), AKT (sc-8312), G₅ α (sc-823), peroxisome proliferator-activated receptor α (PPAR α ; sc-9000) (all Santa Cruz Biotechnology, Santa Cruz, CA), pS473-AKT (no. 9271), uncoupling protein 1 (UCP1; no. 14670), adipose triglyceride lipase (ATGL; no. 2439), pSer563-HSL (no. 4139), pSer660-HSL (no. 4126), hormone-sensitive lipase (HSL; no. 4107), pPKA substrate (RRXS*/T*; no. 9624) (all Cell Signaling Technology, Danvers, MA) and β -actin (A1978; Sigma-Aldrich) were used.

Plasma Liquid Chromatography–Mass Spectrometry Metabolomics

Animals were anesthetized with ketamine/xylazine (i.p., 100 mg/kg and 10 mg/kg, respectively) or CO₂ inhalation. Blood was drawn (500–700 μ L) via cardiac puncture, filled into lithium-heparin- or EDTA-coated tubes (Greiner Bio-One, Kremsmünster, Austria), and centrifuged in <30 min after collection (15 min, 7,000 rpm, 4°C). Plasma was snap frozen and stored at –80°C.

Metabolites were analyzed by targeted liquid chromatography (LC)–high resolution mass spectrometry (MS) metabolomics according to Bajad et al. (22) by hydrophilic interaction LC at the HEALTH Institute for Biomedicine and Health Sciences, JOANNEUM RESEARCH (Graz, Austria) as described previously (23). Samples were processed according to Yuan et al. (24). Raw data were converted into mzXML by msConvert (ProteoWizard Toolkit v3.0.5), and metabolites were targeted-searched by the in-house developed tool PeakScout, with a reference list containing accurate mass and retention times in agreement with standards outlined by Sumner et al. (25). Pure substances of all analytes, except lipids, were run on the same system to obtain exact reference retention times and fragmentation spectra. The results for six samples had to be removed from analysis due to considerable outlier behavior in principal component analysis (PCA; two from GR Δ Adip HFD cohort and one from each of the fasted control, fasted GR Δ Adip, fed control, and GR Δ Adip cohorts).

Statistical Analyses

Statistics were performed with GraphPad Prism or R (26) (v3.2.1, packages *stats*, *missMDA*, and *nlme*) using TibcoSpotfire (v7.0.0). All data except LC-MS metabolomics are presented as mean \pm SEM. Two-tailed Student *t* test or Wilcoxon rank-sum test was used for comparing two groups and one-way ANOVA followed by Tukey, Dunns, or Bonferroni post hoc tests for multiple comparison. Tolerance tests and body growth curves were analyzed with repeated-measures two-way ANOVA followed by Bonferroni post hoc tests. *P* < 0.05 was considered

statistically significant. Data for EE were analyzed using ANCOVA with body weight and body composition (fat and lean mass) as covariates as previously suggested (27). For LC-MS metabolomics, PCA analysis was performed centered and scaled to unit variance (R function *prcomp*). Missing values were imputed by a regularized expectation-maximization (R function *imputePCA* and *estim_ncpPCA*). Log₁₀-transformed data were found to be sufficiently normally distributed according to Kolmogorov-Smirnov (86% of all metabolites were normally distributed) and sufficiently homoscedastic according to Levene (84% of all metabolites were homoscedastic). Differences between independent groups were analyzed by ANOVA (R function *aov*) followed by Benjamini-Hochberg (R function *p.adjust*) post hoc test.

RESULTS

Abnormal Plasma Metabolome in GR Δ Adip Mice

Deletion of *Nr3c1* was confirmed by mRNA and protein expression analyses of inguinal WAT (iWAT), eWAT, and brown adipose tissue (BAT) (Fig. 1A and B). GR Δ Adip mice displayed no overt alterations in weights or morphology of eWAT, iWAT, and BAT compartments (Supplementary Fig. 1A and B). Accordingly, adipogenic markers (*Cebpb*, *Pparg*, and *Fabp4*) and adipocyte-specific genes (*Adiponectin*, *Leptin*, and *Ucp1*) were not differentially expressed among genotypes (Supplementary Table 2).

To initially illustrate the basal metabolic signature of GR Δ Adip mice, plasma samples of ad libitum–fed mice were analyzed by targeted LC-MS metabolomics (Supplementary Table 3; PCA results: Supplementary Fig. 2A). A total of 157 metabolites were of suitable quality for multivariate statistical analysis, 20 metabolites only for univariate statistical analysis. In GR Δ Adip mice compared with controls, 59 metabolites were significantly decreased (*P* < 0.05, ANOVA) and 22 were decreased by trend (0.05 < *P* < 0.1, ANOVA). The majority of decreased metabolites were related to fatty acid (FA)/lipid metabolism (46, most pronounced in long-chain FA), amino acid (AA) metabolism (14, mainly proteogenic and branched-chain AAs, which have been implicated as independent risk factors for diabetes [28]), and nucleotide metabolism (10, mainly pyrimidine metabolites) (Fig. 1C and Supplementary Table 3). This demonstrates a considerable impact of adipocyte GR deficiency on the plasma metabolome and, thus, systemic substrate partitioning, which likely affects whole-body glucose and lipid metabolism in GR Δ Adip mice (6,29).

Reduced Lipolytic and Gluconeogenic Capacity in GR Δ Adip Mice

First, we analyzed glucose homeostasis in GR Δ Adip mice. In 4 h– and 16 h–fasted mice, blood glucose and plasma insulin levels were not significantly altered (Fig. 2A). GTTs revealed no differences in glucose clearance between the genotypes (Supplementary Fig. 2B). The hypoglycemic response during ITTs was similar in both genotypes (Fig. 2B), whereas blood glucose starting from 30 min after

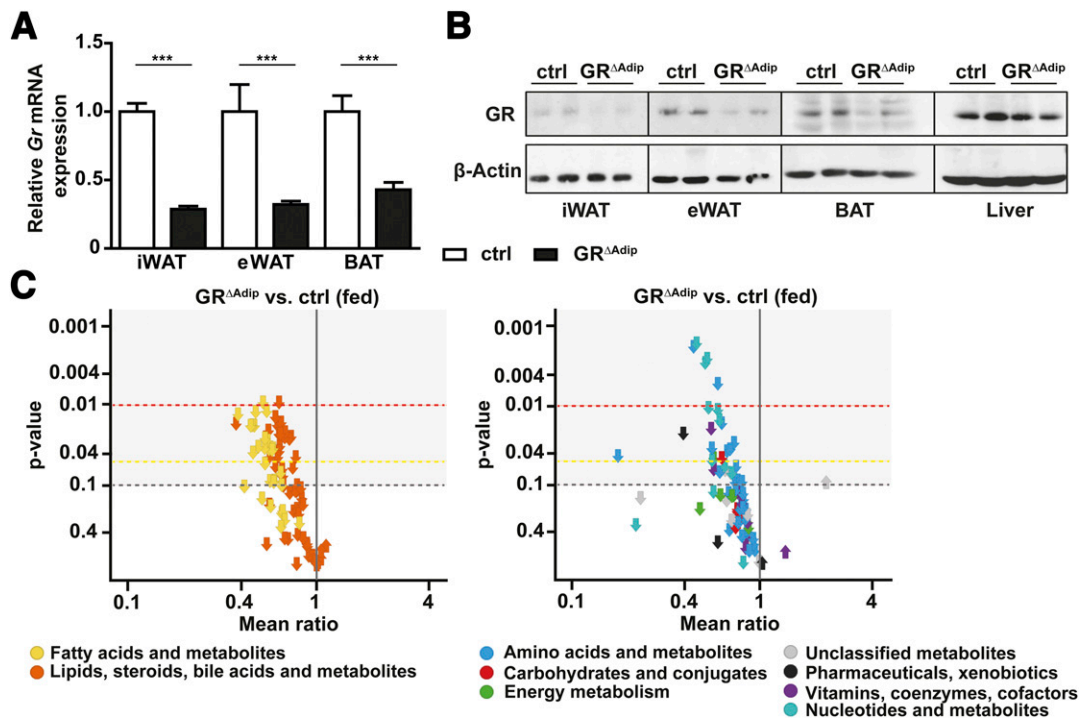


Figure 1—Basal metabolic signature in plasma of $GR^{\Delta Adip}$ mice. **A**: Relative mRNA expression of *Gr* as determined by qRT-PCR in total iWAT, eWAT, and BAT of 10- to 12-week-old ad libitum-fed control (ctrl) and $GR^{\Delta Adip}$ mice. Ct values were normalized to *Actb* ($n = 4-7$ /genotype). **B**: Representative Western blot of GR expression in total iWAT, eWAT, BAT, and liver protein extracts of ad libitum-fed ctrl and $GR^{\Delta Adip}$ mice. **C**: Volcano plots of relative abundance ratios of metabolites in plasma of ad libitum-fed $GR^{\Delta Adip}$ compared with ctrl mice as detected by LC-MS ($n = 5-6$ /genotype). Each arrow represents an individual metabolite within the indicated metabolite classes, and the direction of the arrow indicates if the metabolite is increased or decreased. Respective *P* values are plotted on the y-axis. Data are shown as the mean \pm SEM. ****P* < 0.001. For all analyses: 8-week-old male mice and standard diet ad libitum.

insulin administration was lower in $GR^{\Delta Adip}$ mice. This delay in posthypoglycemic recovery suggests a reduction in counter-regulatory mechanisms such as hepatic glucose production (HGP). Insulin-induced AKT phosphorylation (Ser473) was greater in $GR^{\Delta Adip}$ livers than in controls (Fig. 2C). This was associated with a lower TG content in $GR^{\Delta Adip}$ livers (Fig. 2D). Suppression of WAT lipolysis can indirectly reduce HGP by decreasing the influx of glycerol and NEFA (30). In the absence and presence of insulin, NEFA release from eWAT explants of 4 h-fasted $GR^{\Delta Adip}$ mice was clearly reduced compared with controls (Fig. 2E). Yet, consistent with a comparable insulin-stimulated AKT phosphorylation in eWAT (Fig. 2C), insulin-mediated suppression of lipolysis was similar between genotypes (49% vs. 51%). NEFA release from 16 h-fasted $GR^{\Delta Adip}$ eWAT explants was also reduced, which was mirrored in decreased plasma NEFA (indicator for WAT lipolysis) and blood β -ketones (indicator for hepatic FA oxidation [FAO]) in 16 h-fasted $GR^{\Delta Adip}$ mice (Fig. 2F). Blood glucose levels of 16 h-fasted $GR^{\Delta Adip}$ mice during PTTs were lower compared with controls (Fig. 2G), reflecting reduced glucose production from the carbon precursor pyruvate. Thus, the lipolytic capacity of $GR^{\Delta Adip}$ mice is diminished, which correlates with a decrease in glucose production (Supplementary Fig. 2C).

Reduced Thermogenesis in $GR^{\Delta Adip}$ Mice

Thermogenesis in BAT requires mobilization of lipid stores, induction of β -oxidation, and mitochondrial uncoupling. To evaluate BAT functionality upon adipocyte GR deficiency, we subjected mice to a brief 4-h fast followed by a 4-h exposure to 4°C. Body temperatures of $GR^{\Delta Adip}$ were slightly higher when housed at 23°C (4-h fast; $P = 0.072$), whereas their ability to maintain stable body temperatures at 4°C was mildly reduced (Fig. 3A). Despite the impaired cold adaptation, UCP1 and PPAR α levels were similar in BAT of cold-exposed $GR^{\Delta Adip}$ and control mice (Fig. 3B). While BAT uses FA stores to fuel thermogenesis, WAT provides energy in the form of FA for utilization in BAT. The histology of BAT revealed no differences between genotypes when housed at 23°C (Supplementary Fig. 1B). Yet, upon cold exposure, the amount of lipid droplets decreased to a higher extent in GR-deficient BAT (Fig. 3C), suggesting that BAT lipolysis is not impaired. In contrast, plasma NEFA and β -ketone concentrations, indicators of WAT lipid mobilization and redistribution, were reduced in cold-exposed $GR^{\Delta Adip}$ mice (Fig. 3D). Considering the requirement of external FA supply for BAT-mediated temperature maintenance (31), these data suggest that the reduced cold-induced thermogenesis is related to impaired WAT lipolysis and NEFA flux.

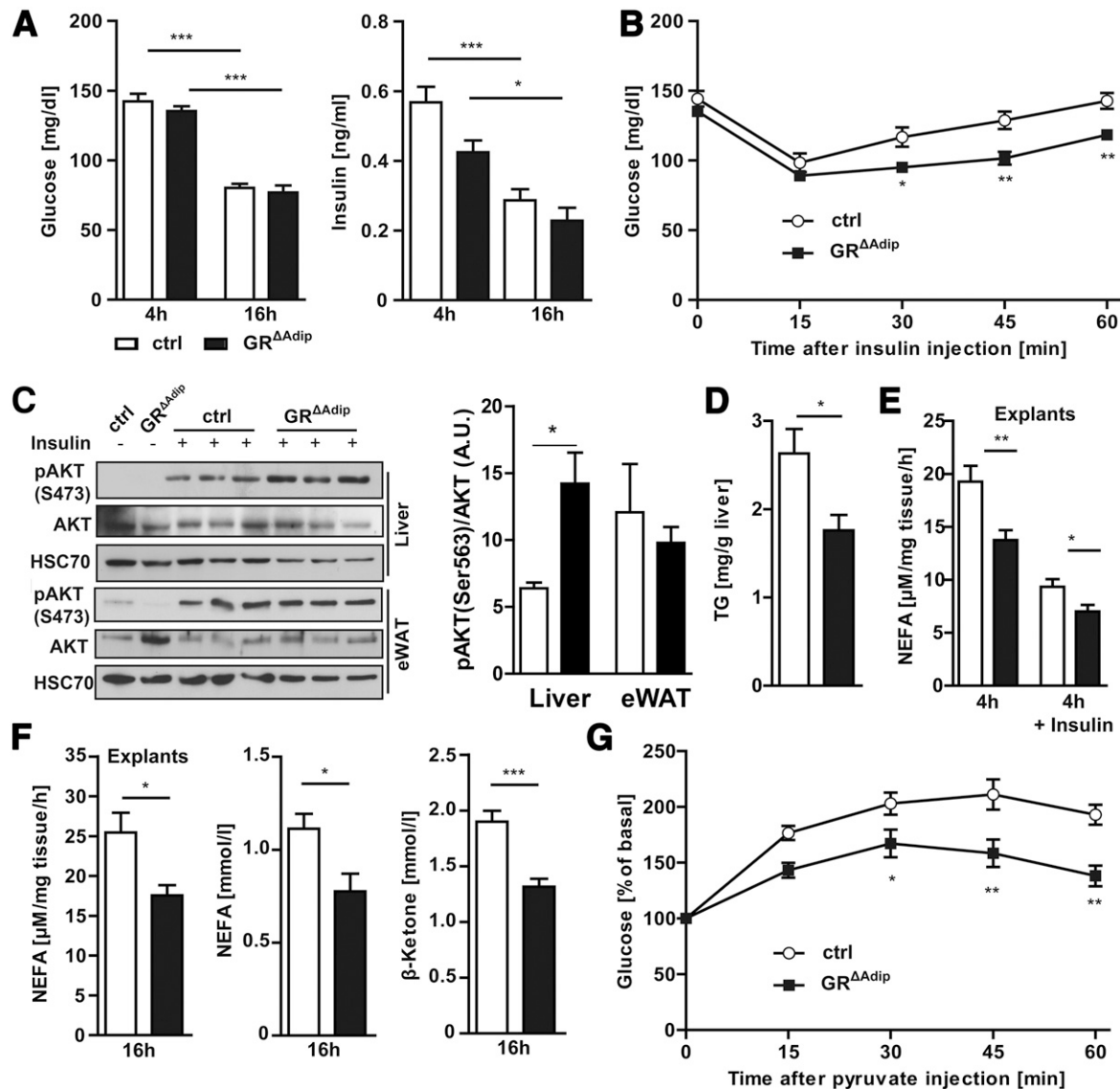


Figure 2—Reduced lipolytic and gluconeogenic capacity in GR^{ΔAdip} mice. **A**: Fasting blood glucose and plasma insulin level at indicated time points. Insulin concentrations were determined by ELISA ($n \geq 6$ /genotype). **B**: ITT. After a 4-h fast, insulin was administered through intraperitoneal injection (0.75 units/kg body weight; $n = 9$ /genotype). Blood glucose levels were determined at indicated time points. **C**: Representative Western blot analysis and quantification of insulin-stimulated phosphorylation of AKT in liver and eWAT (0.75 units/kg body weight). HSC70 was used as a loading control (ctrl). Protein bands were quantified by densitometry, and total protein expression was corrected for the respective loading control ($n = 3$ /genotype). **D**: Total liver TG content in ad libitum-fed mice as determined by a colorimetric assay ($n \geq 6$ /genotype). **E**: NEFA release from eWAT explants of 4 h-fasted mice in absence or presence of insulin (30 ng/mL; $n \geq 2$ mice/genotype/treatment; $n = 10$ explants/genotype). **F**: NEFA release from eWAT explants of 16 h-fasted mice ($n \geq 2$ mice/genotype/treatment; $n = 10$ explants/genotype). Plasma NEFA and blood β -ketone level of 16 h-fasted mice. Parameters were determined by colorimetric assays ($n \geq 6$ /genotype). **G**: Pyruvate tolerance test through intraperitoneal injection of pyruvate (2 g/kg body weight) after a 16-h fast ($n \geq 7$ /genotype). Blood glucose levels were determined at indicated time points. For **B** and **G**, results are from two to three independent experiments. Data are shown as the mean \pm SEM. * $P < 0.05$; ** $P < 0.01$; *** $P < 0.001$. For all analyses: 8-week-old male mice and standard diet ad libitum.

Attenuated Aging-Associated Obesity and Hepatic Steatosis in GR^{ΔAdip} Mice

Progressing age is linked to abnormalities of carbohydrate and lipid metabolism. Thus, we analyzed whether GR deficiency would lead to beneficial metabolic effects at older age. Aging-associated weight gain was attenuated in GR^{ΔAdip} mice (Fig. 4A) and body fat was reduced compared with controls at 52 weeks of age (Fig. 4B). Accordingly,

GR^{ΔAdip} mice had smaller WAT compartments (Fig. 4C), in which adipocyte hypertrophy was less frequently observed (Supplementary Fig. 3A). GR^{ΔAdip} mice that were 4 h fasted displayed lower blood glucose levels and presented an overall reduction of total TG, cholesterol, NEFA, and β -ketones in the circulation, whereas corticosterone levels were comparable between genotypes (Supplementary Fig. 3B). Weights of GR^{ΔAdip} livers were reduced

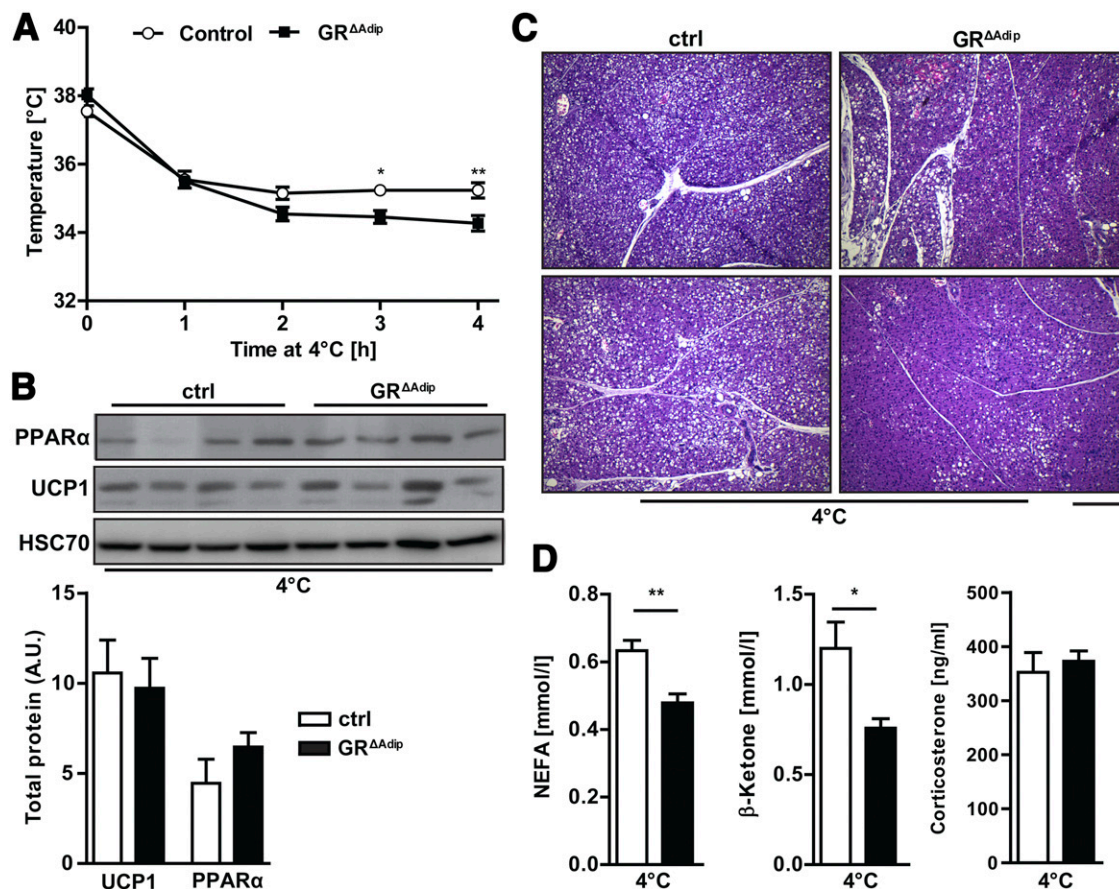


Figure 3—Reduced thermogenesis in GR^{ΔAdip} mice. **A**: Body temperatures of GR^{ΔAdip} and control (ctrl) mice upon acute exposure to 4°C for the indicated time ($n \geq 6$ /genotype). **B**: Western blot analysis and quantification of UCP1 and PPAR α protein levels in BAT of 4-h cold-exposed mice. HSC70 was used as a loading control. Protein bands were quantified by densitometry, and total protein expression was corrected for the respective loading control ($n = 4$ /genotype). **C**: Representative H-E staining of BAT sections from GR^{ΔAdip} and ctrl mice after 4 h of cold exposure. Scale bar indicates 200 μ m. **D**: Plasma NEFA, corticosterone, and blood β -ketone level of 4-h cold-exposed mice. NEFA was determined by colorimetric assays and corticosterone was measured by ELISA ($n \geq 6$ /genotype). Data are shown as the mean \pm SEM. * $P < 0.05$; ** $P < 0.01$.

(Fig. 4C) and steatosis scores of $>5\%$ were found only in control livers (Fig. 4D).

To further characterize the phenotype of aged GR-deficient mice, we determined their metabolic parameters in a PhenoMaster metabolic cage system. GR^{ΔAdip} mice had higher RER during light and dark cycles, indicating an overall preference for carbohydrates as metabolic substrate. Locomotor activity, EE, and food intake were not significantly different between genotypes (Fig. 4E and Supplementary Fig. 3C), although GR^{ΔAdip} mice consumed a slightly higher amount of food. There was no significant effect of GR deficiency on EE after ANCOVA with body weight or lean or fat mass as covariate (data not shown). These data indicate that neither increased physical activity/metabolic rates nor decreased food intake are determinants of reduced adiposity in aged GR^{ΔAdip} mice. However, we cannot fully exclude subtle increases in daily EE and/or locomotor activity that might have contributed to reduced fat mass gain during the aging process.

Reduced HFD-Induced Obesity, Improved Glucose Tolerance, and Hepatic Steatosis in GR^{ΔAdip} Mice

To investigate whether reduced susceptibility to metabolic dysfunctions also occurs upon diet-induced obesity, mice were subjected to HFD feeding for 20 weeks. HFD-fed GR^{ΔAdip} mice gained significantly less weight than HFD-fed controls, despite similar cumulative food intake (Fig. 5A and Supplementary Fig. 4A). Reduced weight gain manifested early in HFD-fed GR^{ΔAdip} mice (Fig. 5A), accompanied by lower levels of several circulating FA species and a trend toward reduced plasma NEFA (Supplementary Table 3 and Supplementary Fig. 4B). After 2 weeks of HFD feeding, mRNA expression of several genes critical for FA storage were either significantly reduced or reduced by trend in GR^{ΔAdip} eWAT compared with controls (acyl-CoA carboxylase [*Acaca*], glycerol-3-phosphate acyltransferase 3 [*Gpat3*], diacylglycerol-acyltransferase-2 [*Dgat2*], phosphoenolpyruvate carboxykinase [*Pck1*], and FA transport protein 1 [*Slc27a1*]) (Fig. 5B). *Acaca* and *Pck1* mRNA levels showed a similar trend in GR-deficient iWAT, whereas there was no

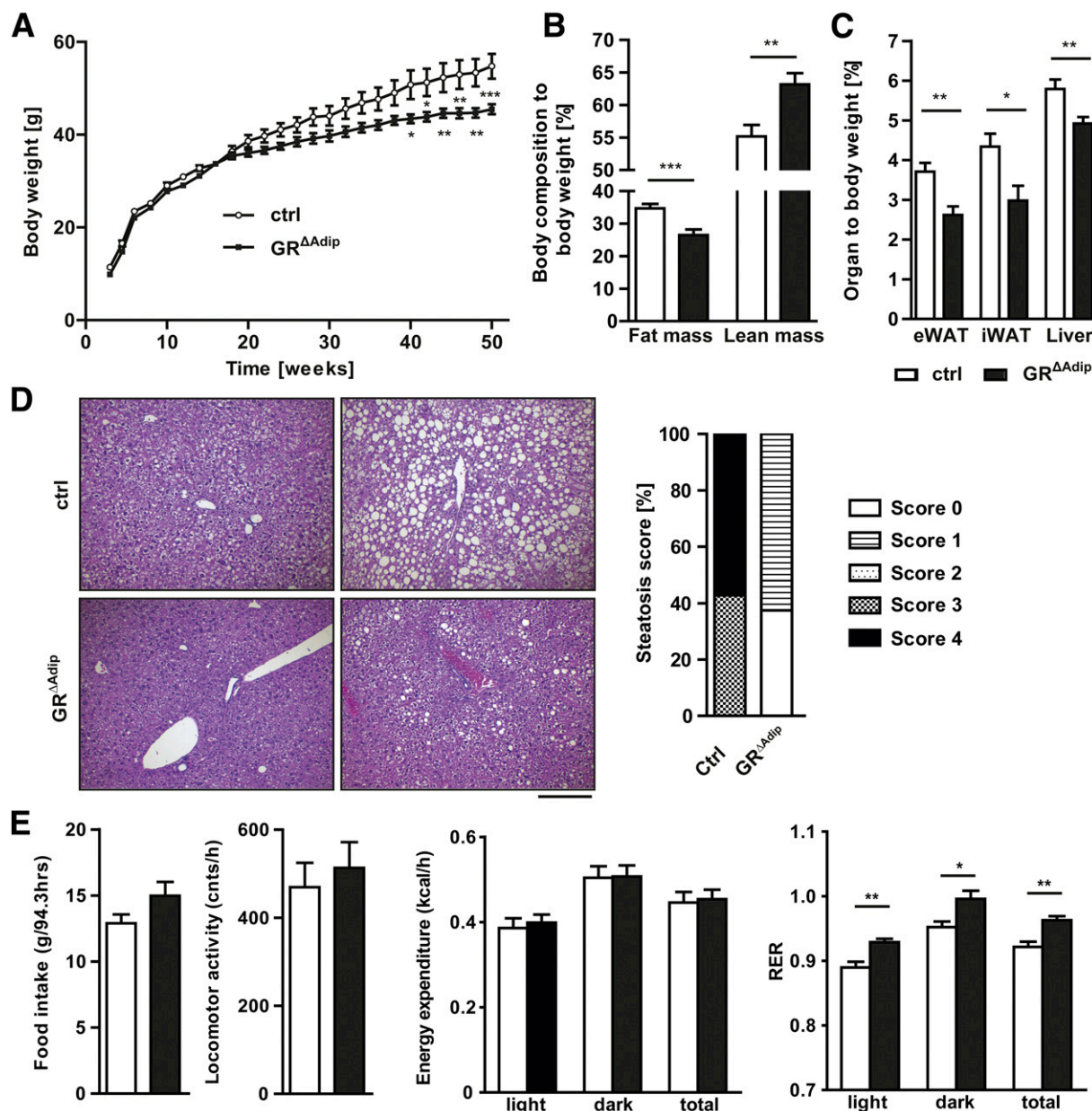


Figure 4—Attenuated aging-associated obesity and hepatic steatosis in adipocyte GR-deficient mice. **A**: Postnatal body weight gain of GR^{ΔAdip} mice and control (ctrl) littermates ($n = 12$ /genotype; four independent litters). **B**: Noninvasive monitoring of body compositions of 52-week-old GR^{ΔAdip} and ctrl mice using EchoMRI. Total body fat and lean mass are depicted in relation to body weight ($n = 10$). **C**: Wet weight of eWAT, iWAT, and liver in relation to body weight of 52-week-old mice ($n \geq 7$ /genotype). **D**: Representative H-E stainings of livers and quantification of steatosis scores at 52 weeks of age ($n \geq 7$ /genotype). Score 1, <5%; score 2, 5–20%; score 3, >20%; score 4, >50%. Scale bar indicates 200 μ m. **E**: Cumulative food intake, daily locomotor activity, EE, and RERs of aged mice ($n \geq 6$ /genotype). For all analyses, mice were fed a standard diet ad libitum; data are shown as the mean \pm SEM. * $P < 0.05$; ** $P < 0.01$; *** $P < 0.001$.

change in expression of FA synthase (*Fasn*) and the FA transporter *Cd36* (platelet glycoprotein 4) in both WAT compartments. At termination, HFD-fed GR^{ΔAdip} mice displayed lower WAT weights than HFD-fed controls (Supplementary Fig. 4C), and μ -CT analysis confirmed significantly decreased subcutaneous and visceral fat volume of GR^{ΔAdip} mice (Fig. 5C). Accordingly, adipocyte hypertrophy in GR^{ΔAdip} eWAT and iWAT was reduced

(Fig. 5D and Supplementary Fig. 4D). Consistent with the aging cohort, plasma corticosterone levels were not significantly different between HFD-fed control and GR-deficient mice (Supplementary Fig. 4E).

Next, we asked whether GR deficiency improves deteriorated glucose metabolism associated with HFD. Blood glucose levels trended lower in HFD-fed GR^{ΔAdip} mice compared with controls (Fig. 6A), and their fasting

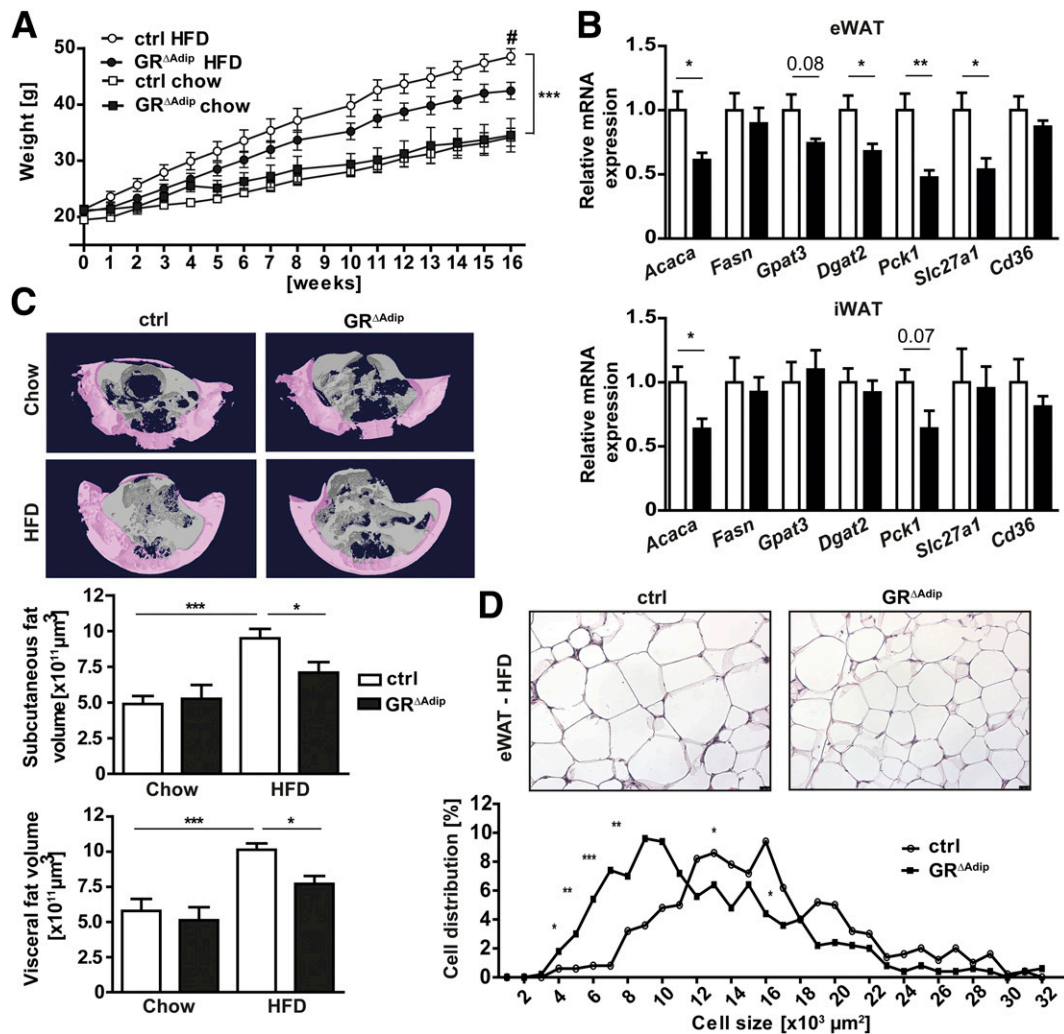


Figure 5—Adipocyte-specific GR-deficient mice gain less weight under HFD conditions. Mice from each genotype received either a chow diet or an HFD starting at weeks 3–5 after birth. **A:** Weight gain of control (ctrl) and GR^{ΔAdip} littermates over a time period of 16 weeks ($n = 5–10$ /genotype). **B:** Relative mRNA expression of genes critical for lipid storage in eWAT and iWAT as determined by qRT-PCR of HFD-fed ctrl and GR^{ΔAdip} mice. Ct values were normalized to *Actb* ($n \geq 5$ /genotype). **C:** Three-dimensional models of subcutaneous (pink) and visceral (gray) fat in the abdominal region of chow diet- or HFD-fed mice. Quantification of subcutaneous and visceral fat volume after HFD or chow diet of the indicated genotypes ($n = 5–10$ /genotype). **D:** Representative H-E staining of eWAT and quantification of adipocyte cell size from eWAT of ctrl and GR^{ΔAdip} mice after HFD ($n = 5$ /genotype). Scale bar indicates 25 μm . Data are shown as the mean \pm SEM. * $P < 0.05$; ** $P < 0.01$; *** $P < 0.001$; # $P < 0.05$ (GR^{ΔAdip} HFD vs. ctrl HFD).

plasma insulin levels were significantly lower (Fig. 6B). In agreement, HOMA-IR was decreased in HFD-fed GR^{ΔAdip} mice, suggesting improved insulin sensitivity (Fig. 6C). Consistent with the lower HOMA-IR, systemic glucose tolerance of HFD-fed GR^{ΔAdip} mice was improved compared with obese controls (Fig. 6D), and insulin-stimulated AKT phosphorylation (Ser473) in muscle, eWAT, and liver of HFD-fed GR^{ΔAdip} mice was increased (Fig. 6E and Supplementary Fig. 4F).

Similar to the aging cohort, adipocyte GR deficiency attenuated HFD-induced hepatic lipid accumulation and liver weights, which was reflected in lower steatosis scores (Fig. 6F and G). Hepatic mRNA expression of *Fasn* and *Gpat1*, two rate-limiting enzymes of lipogenesis, was reduced in HFD-fed GR^{ΔAdip} mice, accompanied by diminished

expression of *Pparg* and two FA transporters, *Cd36* and *Slc27a4* (long-chain FA transport protein 4) (Fig. 6H). This suggests that decelerated FA uptake and lipogenesis might contribute to lower steatosis scores in GR-deficient mice. Thus, adipocyte GR deficiency reduces obesity, diminishes hepatic steatosis, and improves glucose tolerance in HFD-fed mice.

Impaired Lipolysis Disrupts the Feeding-Fasting Transition in GR^{ΔAdip} Mice

Having demonstrated that adipocyte GR promotes metabolic dysfunctions in aged and fat-fed mice, we lastly evaluated the requirement of adipocyte GR for energy homeostasis under prolonged fasting conditions. Upon 48-h fasting, total body weight loss was similar among

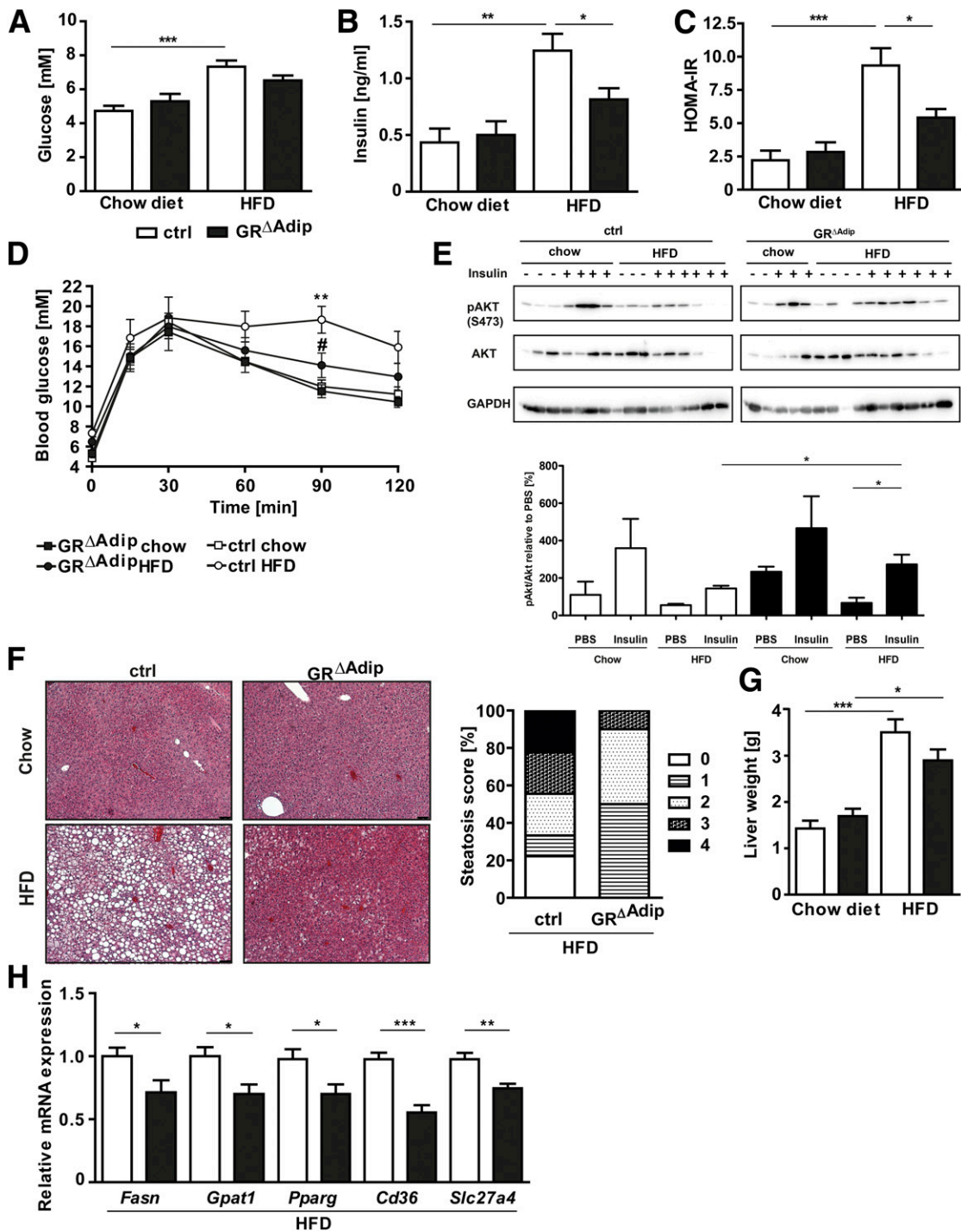


Figure 6—Adipocyte-specific GR loss improves glucose tolerance and hepatic steatosis under HFD conditions. **A**: Blood glucose levels of 12 h-fasted control (ctrl) and GR^{ΔAdip} mice ($n = 5-10$ mice/genotype). Plasma insulin levels (**B**) and HOMA-IR (**C**) of 12 h-fasted ctrl and GR^{ΔAdip} mice ($n = 5-10$ mice/genotype). Insulin concentrations were determined by ELISA. **D**: GTT 18 weeks after chow/HFD. Glucose was administered by intraperitoneal injection (2 g/kg body weight) after a 16-h fast. Blood glucose levels were determined at indicated time points ($n = 5-10$ /genotype). **E**: Western blot analysis of insulin-stimulated phosphorylation of AKT in muscle (1 unit/kg body weight) from ctrl and GR^{ΔAdip} mice after chow or HFD. **F**: Representative H-E staining of liver sections from ctrl and GR^{ΔAdip} mice after chow or HFD and histopathological characterization of liver phenotypes from HFD mice ($n \geq 9$ /genotype). Steatosis score 1, <5%; score 2, 5–20%; score 3, >20%; score 4, >50%. Scale bar indicates 25 μ m. **G**: Comparison of wet weight of liver after chow and HFD of the indicated genotypes ($n = 5-10$ mice/genotype). **H**: Relative mRNA expression of *Fasn*, *Gpat1*, *Pparg*, *Cd36*, and *Slc27a4* in liver as determined by qRT-PCR of HFD-fed ctrl and GR^{ΔAdip} mice. Ct values were normalized to *Actb* ($n = 8-10$ /genotype). For all analyses, ctrl and GR^{ΔAdip} mice received either a chow diet or an HFD for 18–20 weeks starting at weeks 3–5 after birth; data are shown as the mean \pm SEM. * $P < 0.05$; ** $P < 0.01$; *** $P < 0.001$; # $P < 0.05$ (GR^{ΔAdip} HFD vs. ctrl HFD).

genotypes (Supplementary Fig. 5A). Notably, all mice survived 48-h fasting and did not present symptoms of a hypoglycemic shock (i.e., trembling, seizures, or unconsciousness). Body fat mass was approximately twofold higher in fasted $GR^{\Delta Adip}$ mice compared with controls, whereas their lean mass was decreased (Fig. 7A). Accordingly, $GR^{\Delta Adip}$ WAT compartments were enlarged, whereas their gastrocnemius, heart, and liver weights were reduced (Supplementary Fig. 5B). Consistent with their preserved fat mass, $GR^{\Delta Adip}$ mice presented increased adipocyte sizes, lower plasma NEFA and glycerol concentrations, decreased hepatic TG accumulation, and reduced circulating TG levels (Fig. 7B and C, Supplementary Fig. 1B, and Supplementary Fig. 5C and D). Blood β -ketones were substantially lower (Fig. 7C), indicating reduced FAO and ketogenesis. Hepatic PPAR α and FGF21 are key mediators of fasted states and contribute to lipid utilization by increasing FAO in liver (32). Fasting-induced upregulation of *Ppara* and *Fgf21* mRNA expression was impaired in $GR^{\Delta Adip}$ livers, accompanied by decreased plasma FGF21 levels (Fig. 7D and Supplementary Fig. 5E). In contrast to shorter fasting periods, 48-h fasting blood glucose was unexpectedly increased in $GR^{\Delta Adip}$ mice compared with controls (Fig. 7C), suggesting that the observed breakdown of lean mass might provide substrates for glucose production. In support of this assumption, circulating corticosterone, which potently induces protein catabolism and HGP (1), increased to a higher extent in 48 h- but not in 16 h-fasted $GR^{\Delta Adip}$ mice (Fig. 7E). Additionally, fasting-induced upregulation of gluconeogenic genes *Pgc1a* and *Pck1* was similar in livers of both genotypes (Supplementary Fig. 5F). To characterize the fasting metabolome of $GR^{\Delta Adip}$ mice in more detail, plasma samples were analyzed by targeted LC-MS. From 177 metabolites, 42% were significantly different in 48 h-fasted compared with fed $GR^{\Delta Adip}$ mice (Fig. 7F and Supplementary Table 3). Strong increases in AAs and related metabolites, several FA species, and nucleotides were observed. Conversely, in fasted controls, abundance of most AAs and nucleotides was either unchanged or lower than in fed controls. Eighteen percent of metabolites were significantly different between 48 h-fasted $GR^{\Delta Adip}$ mice and controls. These included hexose, pentose, nucleotides, and AAs, all of which, in contrast to the fed state, displayed a greater quantity in $GR^{\Delta Adip}$ mice (Fig. 1C, Fig. 7F, and Supplementary Table 3). This reveals that the GR in adipocytes is indispensable for normal substrate mobilization and energy metabolism under prolonged fasting conditions.

Dysregulation of Lipolytic Signaling in $GR^{\Delta Adip}$ Mice

To determine the molecular underpinning of impaired lipolysis, we compared mRNA and protein expression of lipolytic key factors in eWAT of fed and 48 h-fasted mice. HSL (*Lipe*) mRNA levels were similar among genotypes, whereas upregulation of ATGL (*Pnpla2*) and CGI58 (comparative gene identification 58; *Abhd5*) mRNA

expression was significantly reduced in fasted $GR^{\Delta Adip}$ eWAT (Fig. 8A). The protein level of ATGL and its coactivator CGI58 displayed a similar expression pattern in eWAT of fasted mice (Fig. 8B). Fasting-induced lipolysis requires cAMP-mediated activation of protein kinase A (PKA) with subsequent phosphorylation of HSL and perilipin, thereby indirectly activating ATGL via release of CGI58 (33). Upon fasting, total PKA substrate phosphorylation including HSL (Ser563/660) and perilipin was substantially decreased in $GR^{\Delta Adip}$ eWAT (Fig. 8B and C). Thus, we analyzed mRNA expression of genes critical for β -adrenergic activation of PKA. Expression of the inhibitory α 2-adrenergic receptor (α 2-AR) and inhibitory G-protein α -subunit isoforms was similar between genotypes (Supplementary Fig. 6A), whereas upregulation of β 2-AR (*Adrb2*) was reduced in $GR^{\Delta Adip}$ eWAT under fasting conditions. Conversely, β 3-AR (*Adrb3*) mRNA levels were increased (Fig. 8D). Notably, fasting-induced upregulation of the stimulatory G-protein α -subunit ($G_s\alpha$; *Gnas*), which couples β -ARs to adenylate cyclase-mediated production of intracellular cAMP (34), was significantly diminished in GR-deficient eWAT (Fig. 8D and E). To functionally identify the GR-dependent signaling step in β -adrenergic signal transduction, we applied pharmacological agonists on eWAT explants from 16 h-fasted mice. GR deficiency reduced cAMP generation upon treatment with isoproterenol (nonselective β -adrenergic agonist) but not in response to forskolin (direct adenylate cyclase agonist) (Fig. 8F). NEFA release from $GR^{\Delta Adip}$ explants was decreased in response to isoproterenol, CL-316,243 (β 3-AR agonist), and formoterol (β 2-AR agonist), whereas forskolin-stimulated lipolysis was similar between both genotypes (Fig. 8G). Similar results were obtained from isoproterenol- or forskolin-treated eWAT explants of fed $GR^{\Delta Adip}$ mice (Supplementary Fig. 6B), albeit the defect in lipolysis was less pronounced than in 16 h-fasted mice. These data demonstrate that the GR is a pivotal permissive factor for β -adrenergic signal transduction to adenylate cyclase and concomitant activation of the lipolytic cascade in WAT.

DISCUSSION

Our study provides the first genetic evidence for the GR in adipocytes as a critical component in normal and pathophysiological energy metabolism. Initial plasma metabolomics revealed a marked global effect of GR deficiency on systemic metabolite abundance, including a reduction in various FA species and proteogenic/branched-chain AAs (valine, leucine, and isoleucine). Albeit steady-state analysis of plasma represents a static net-balance between metabolite production and consumption, the broad changes indicate that systemic fuel partitioning is partly controlled by GR in adipocytes. Along this line, the diminished gluconeogenic capacity of $GR^{\Delta Adip}$ mice during ITT/PTT may be due to increased hepatic responsiveness to insulin but could also result from a decrease in substrate availability (6). GC exposure

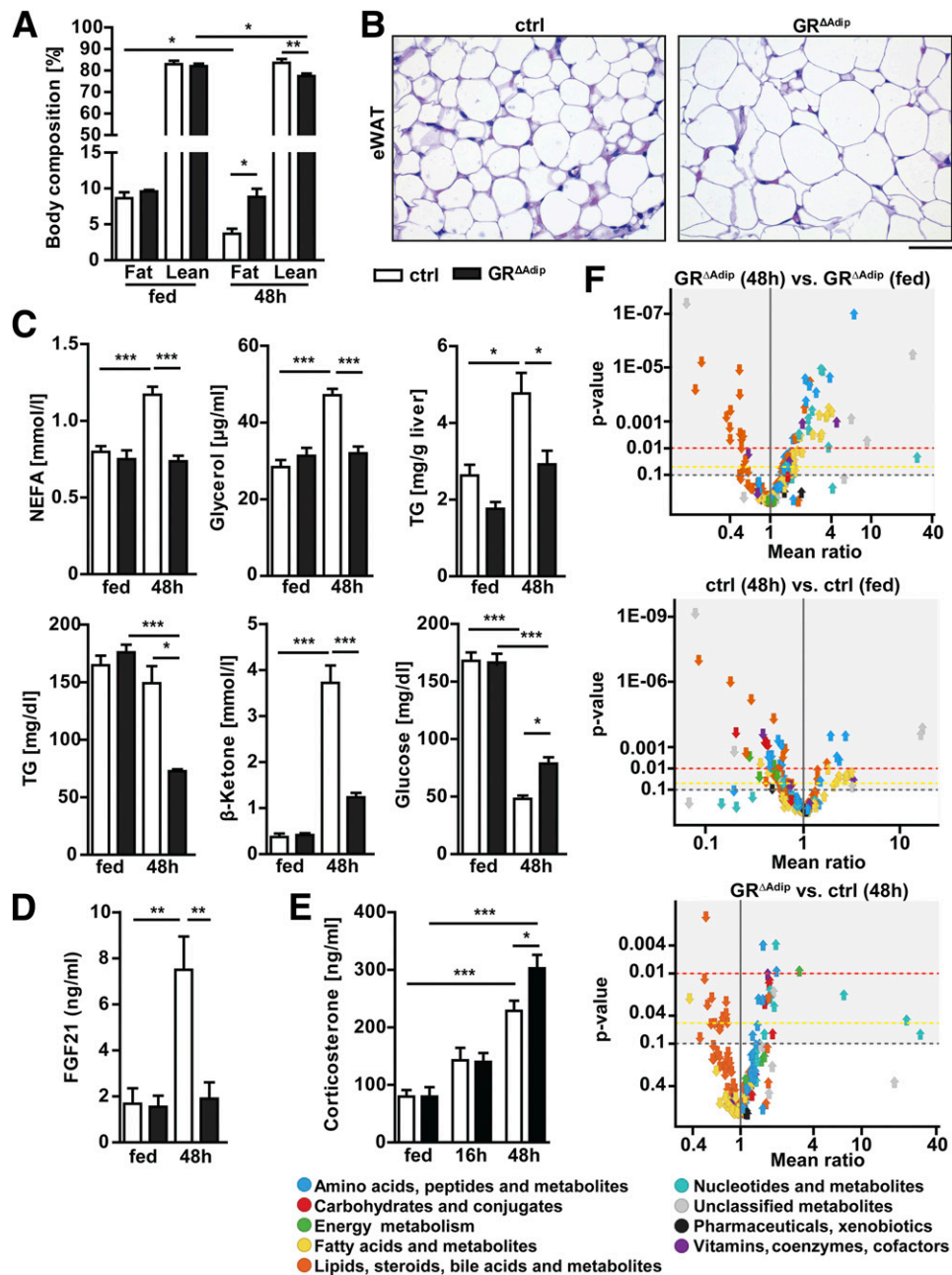


Figure 7—Impaired lipolysis in WAT of GR^{ΔAdip} mice results in aberrant substrate metabolism and lean mass wasting under prolonged fasting conditions. **A**: Noninvasive monitoring of body compositions in fed and 48 h-fasted mice using EchoMRI. Total body fat and lean mass are depicted in relation to body weight ($n = 6/\text{genotype}$). **B**: Representative H-E staining of eWAT from 48 h-fasted mice. Scale bar indicates 50 μm . **C**: Plasma NEFA, glycerol and TG level, liver TG content, blood β -ketone level, and blood glucose of fed and 48 h-fasted mice. Plasma parameters and liver TG were determined by colorimetric assays ($n \geq 6/\text{genotype}$). **D**: Plasma FGF21 level of ad libitum-fed and 48 h-fasted GR^{ΔAdip} and control (ctrl) mice as determined by ELISA. **E**: Plasma corticosterone level of ad libitum-fed, 16 h- and 48 h-fasted GR^{ΔAdip}, and ctrl mice as determined by ELISA. **F**: Volcano plots depicting relative abundance ratios of metabolites as detected by LC-MS metabolomics in plasma of the following groups: 48 h-fasted compared with fed GR^{ΔAdip} mice, 48 h-fasted compared with fed ctrl mice, and 48 h-fasted GR^{ΔAdip} compared with ctrl mice ($n = 5\text{--}6/\text{genotype}$). Each arrow represents an individual metabolite within the indicated metabolite classes, and the direction of the arrow indicates if the metabolite is increased or decreased. Respective P values are plotted on the y-axis. For **A**, **C**, **D**, and **E**, data are shown as the mean \pm SEM. * $P < 0.05$; ** $P < 0.01$; *** $P < 0.001$. For all analyses: 8-week-old male mice and standard diet.

at high concentrations is thought to stimulate lipolysis (1,2). Our data from eWAT explants of 4 h-fasted mice show that the GR is a key factor for lipolysis already in the postabsorptive state. Suppression of WAT lipolysis

correlates with hepatic insulin sensitivity and reduced HGP (34,35) and indirectly counter-regulates gluconeogenesis (6,30,36), as WAT-derived substrate fluxes provide glycerol as direct substrate, and NEFA oxidation promotes

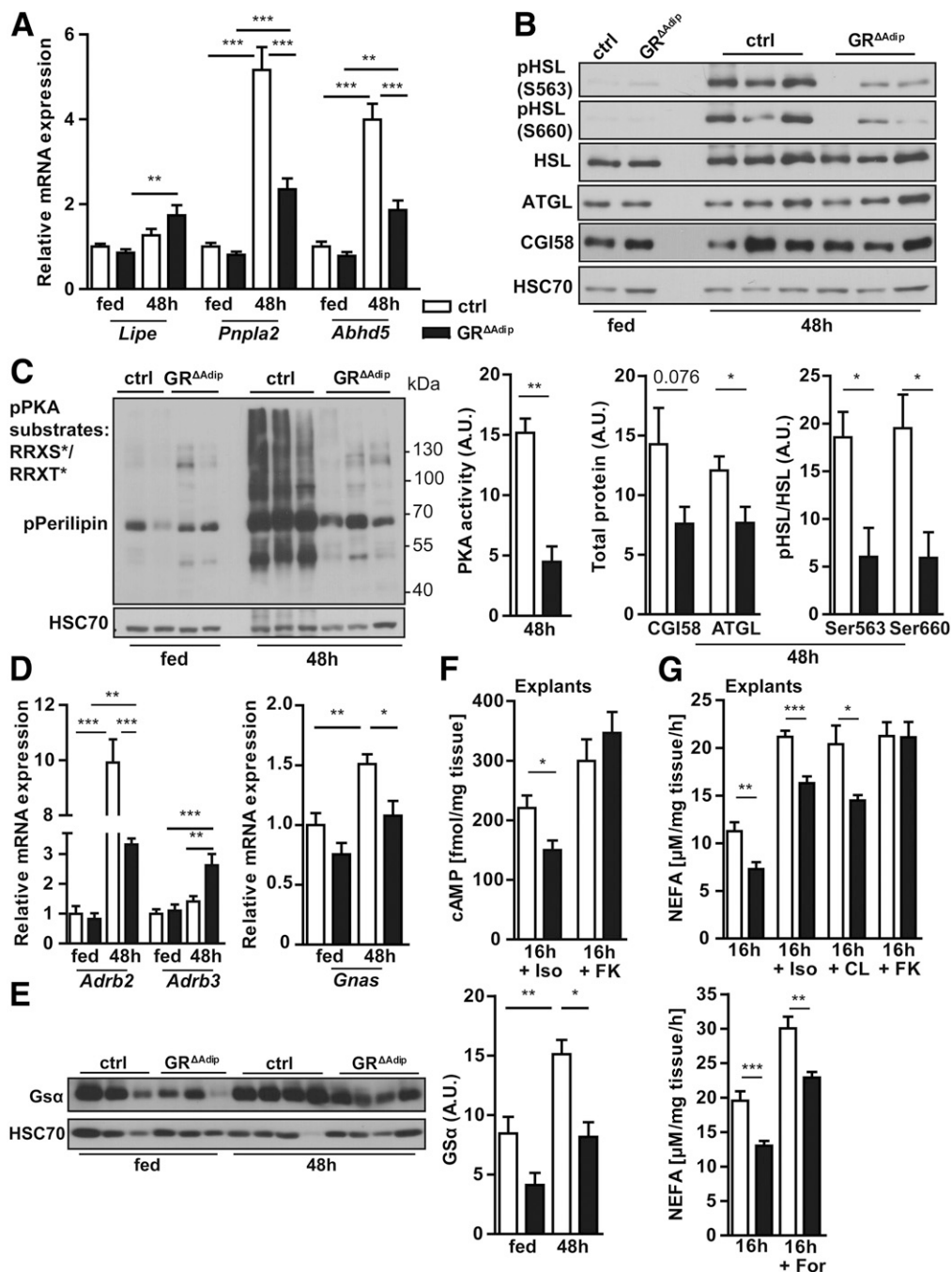


Figure 8—Adipocyte GR deficiency impairs the lipolytic response of white adipocytes through impairment of β -adrenergic signal transduction. **A**: Relative mRNA expression levels of genes with key functions in lipolysis were quantified by qRT-PCR in eWAT under ad libitum feeding and 48-h fasting conditions. Ct values were normalized to *Gapdh* ($n \geq 8$ /genotype). **B**: Representative Western blots of the activation status and/or total protein levels of HSL, ATGL, and CGI58 in eWAT under fed or fasted conditions. HSC70 served as loading control (ctrl). Quantification of CGI58, ATGL expression, and HSL activation status upon fasting ($n = 5$ /genotype). Protein bands were quantified by densitometry; total protein expression was corrected for the respective loading control. **C**: Western blot of eWAT from ad libitum-fed and 48 h-fasted mice using an antibody raised against phosphorylated PKA substrates containing an RRX(S*/T*) epitope motif. Quantification of PKA activity upon fasting ($n = 3$ /genotype). Total phosphorylated PKA substrates were quantified by densitometry and corrected for the respective loading control. **D**: Relative mRNA expression levels of eWAT under ad libitum feeding and 48-h fasting conditions. Ct values were normalized to *Gapdh* ($n \geq 8$ /genotype). **E**: Representative Western blot of $G_{s\alpha}$ in eWAT under fed or fasted conditions. HSC70 served as loading control. Quantification of $G_{s\alpha}$ levels ($n = 5$ /genotype). Protein bands were quantified by densitometry; total protein expression was corrected for the respective loading control. **F**: cAMP level in eWAT explants of 16 h-fasted mice in response to treatment with indicated agonists ($10 \mu\text{mol/L}$; $n \geq 2$ mice/genotype/treatment; $n = 10$ explants/genotype). **G**: NEFA release from eWAT explants of 16 h-fasted mice in absence or presence of indicated agonists ($10 \mu\text{mol/L}$; $n \geq 2$ mice/genotype/treatment; $n = 10$ explants/genotype). Data are shown as the mean \pm SEM. * $P < 0.05$; ** $P < 0.01$; *** $P < 0.001$. For all analyses: 8-week-old male mice and standard diet. CL, CL-316,243; Iso, isoproterenol; FK, forskolin; For, formoterol.

acetyl-CoA-mediated activation of pyruvate carboxylase (37). Therefore, it is conceivable that reduced lipolysis in GR^{ΔAdip} mice contributes in a similar manner to the observed reduction in gluconeogenic capacity.

GC-stimulated lipolysis has been linked to transcriptional upregulation of ATGL and HSL (7,9,38), elevated adenylate cyclase activity (39), intracellular cAMP production, and HSL activation (7,8). Reduced lipolysis in GR^{ΔAdip} mice largely resulted from a block in β -adrenergic activation of PKA and lipolytic downstream signaling (33). The sympathetic nervous system (SNS) regulates induction of WAT lipolysis, and PKA-mediated phosphorylation of HSL serves as surrogate marker for SNS outflow to WAT (40,41). In fasting states, systemic GR antagonism with RU486 decreased β -adrenergic signaling in WAT through suppression of angiopoietin-like 4 (*Angptl4*) (8). However, *Angptl4* expression was not affected in GR^{ΔAdip} eWAT (Supplementary Fig. 6C). GR deficiency decreased the expression of G_s α , which mediates SNS-stimulated lipolysis by transducing signals from β -ARs to adenylate cyclase. Notably, adipocyte-specific deficiency in G_s α blocks WAT lipolysis, mimicking the phenotype of the GR^{ΔAdip} mice (34). In agreement, cAMP generation and NEFA release from GR^{ΔAdip} eWAT explants was reduced in response to β -AR agonists but could be normalized by direct adenylate cyclase agonism. GCs were shown to positively regulate G_s α expression in rat brain (42), suggesting that a similar regulatory mechanism might exist in adipocytes to trigger β -adrenergic lipolytic responses. Accordingly, dexamethasone treatment increased G_s α levels in eWAT of control mice but not in liver or GN muscle, suggesting that the GC-mediated induction of G_s α occurs in a tissue-selective manner (Supplementary Fig. 6D). However, sequence analysis of the corresponding *Gnas* promoter region (NM_201616.2, NM_001077510.4, NM_001310083.1; -3,000 bp of TSS) did not reveal the presence of any sequences likely to act as GC response element. Notably, the GR positively regulates transcription through several mechanisms, including DNA-independent means, by acting as cofactor for lineage-specific transcription factors (43). At this point, however, we cannot predict which molecular mechanism might account for the reduction in *Gnas* expression in GR-deficient WAT, and further molecular studies will be necessary to decipher the underlying causes. Nevertheless, our current data support a model where the GR is required for signal transduction from β 2/3-AR to adenylate cyclase and concomitant induction of lipolysis.

In mice and humans, an increase in GC regeneration by the enzyme 11 β -HSD1 within WAT compartments suggests a role of the GC-GR axis in common obesity (2,12–16). Our findings from aged and HFD-fed GR^{ΔAdip} mice support that suppressing the adipocyte GC-GR axis restricts obesity and its underlying disease state. We observed no differences in EE and/or food consumption that would explain the attenuated obesity of GR^{ΔAdip} mice. Recent studies established an interdependence of lipid mobilization and storage in WAT. Chronic stimulation

of lipolysis was shown to coincide with an upregulation of genes critical for FA storage and induction of de novo lipogenesis in WAT (44). Conversely, blocking lipolysis in chow- and/or HFD-fed mice resulted in downregulation of genes critical for FA storage and in decreased lipogenesis/lipid synthesis in WAT (34,35). Although not functionally proven by our data, the mild, yet collective reduction in several genes related to FA storage in HFD GR^{ΔAdip} WAT suggests that a decrease in lipid synthesis might contribute to the attenuated obesity phenotype. However, further studies are required to determine the exact mechanism(s) underlying the antiobesity effects of adipocyte GR deficiency.

Dysfunctional hypertrophic adipocytes are thought to be in part causative for metabolic dysfunctions upon progressive adiposity (5,45). Improved glucose tolerance and reduced hyperinsulinemia indicate enhanced peripheral responsiveness to insulin in HFD-fed GR^{ΔAdip} mice. Indeed, increased insulin-stimulated AKT phosphorylation was not confined to WAT but also present in muscle and liver of HFD-fed GR^{ΔAdip} mice. As NEFA/lipid accumulation can cause deleterious effects on insulin-sensitive organs (6), and inhibition of lipolysis improves systemic glucose metabolism (34,35), the attenuated adiposity and reduced lipolytic capacity are conceivable possibilities for the ameliorated glucose tolerance in GR^{ΔAdip} mice. Along this line, adipocyte GR deficiency attenuated HFD-induced steatosis. HFD feeding promotes hepatic lipid accumulation partly through upregulation of genes involved in FA uptake and lipid synthesis (46–48), several of which were downregulated in the livers of HFD-fed GR^{ΔAdip} mice. Accordingly, reduced FA influx and endogenous lipid production likely contribute to the attenuation of steatosis in HFD-fed GR^{ΔAdip} mice. Similar to our observations, adipocyte-specific 11 β -HSD1 deletion was shown to ameliorate hypercortisolism-induced glucose intolerance and hepatic steatosis (38). Along with the beneficial metabolic state of the aged GR-deficient cohort, these findings indicate that adipocyte GC-GR activity is involved in the development of systemic metabolic dysfunctions.

In contrast to HFD feeding, adipocyte GR deficiency had adverse consequences when FA became the major energy substrate during prolonged fasting. Fasting induces robust shifts in fuel selection, during which coordinated increases in lipolysis, FAO, and ketogenesis spare glucose and preserve lean mass. Similar to models with impairments in lipolytic enzymes (33,49–51), GR deficiency disrupted the transition to lipid-based energy production (i.e., preserved fat, inefficient FA utilization, and ketogenesis). The simultaneous impaired upregulation of *Ppara* and *Fgf21* in 48 h-fasted GR^{ΔAdip} livers is consistent with a proposed necessity of lipolysis for the expression of both genes (51). FGF21 was shown to be required to sustain fasting hypoglycemia by stimulating corticotropin-releasing hormone in hypothalamic neurons and concomitant release of adrenal corticosterone (52). The increased blood glucose levels in 48 h-fasted GR^{ΔAdip}

mice combined with elevated corticosterone indicate a uniquely different fasting response upon complete FGF21 deficiency versus its scarcity due to defective lipolysis. GCs stimulate lipolysis, lean mass catabolism, AA utilization, and gluconeogenesis (1,4,53). Accordingly, fasting metabolism upon muscle-specific GR deficiency is opposite GR^{ΔAdip} mice in that muscle mass is preserved and WAT depleted (3). Conversely, in fasted GR^{ΔAdip} mice, all tissues except WAT respond to GC, visible as increased circulating AAs (proteogenic and urea cycle related), their metabolites (i.e., 2-ketobutyrate, creatine, creatinine, and carnitine), and glucose (4,53). As gluconeogenesis is intimately connected to the tricarboxylic acid cycle by both substrate supply and energy demand (6,29), lean mass-derived AAs conceivably provided both sources in 48 h-fasted GR^{ΔAdip} mice. The elevation of purine nucleotide precursor and degradation products (i.e., xanthosine, hypoxanthine, xanthine, and urate) additionally suggest that the energetic requirements of the disturbed fasting metabolism in GR^{ΔAdip} mice result in imbalanced ATP synthesis/degradation rates and, thus, a reduction in energy state. Thereby, our results show adipocyte GR as a critical regulator of energy homeostasis during prolonged fasting.

In conclusion, our results demonstrate that the adipocyte GR controls systemic fuel partitioning and energy metabolism. In prolonged fasting states, GR activity is vital to prevent aberrant fuel selection and lean mass wasting by permitting β-adrenergic stimulation of lipolysis and the switch to lipid-based energy production. Conversely, in models of diet- and aging-induced obesity, GR activity is a determinant of systemic metabolic dysfunctions.

Acknowledgments. The authors thank Ute Burret (Institute for Comparative Molecular Endocrinology, University of Ulm) and Safia Zahma (Institute of Animal Breeding and Genetics, University of Veterinary Medicine Vienna) for excellent technical assistance, and the animal facility staff at the University of Ulm, Medical University of Vienna, and the University of Veterinary Medicine Vienna for their support.

Funding. This work was supported by the Austrian Science Fund (FWF P26766 to T.S. and SFB F2807-B20 and SFB F4707-B20 to R.M.), the Deutsche Forschungsgemeinschaft (grants Priority Program Immunobone 1468/Tu 220/6-1, 6-2, Collaborative Research Centre 1149/CO2/INST 40/492-1, and DFG-ANR/TU 220/13-1), and the European Union Research and Innovation funding program (FP7 BRAINAGE) to J.P.T. Part of this work was funded by the Österreichische Forschungsförderungsgesellschaft (COMET Program/K1 COMET Competence Center CBmed, Land Steiermark and Land Wien).

The funders had no role in study design, data collection and analysis, decision to publish, or preparation of the manuscript.

Duality of Interest. No potential conflicts of interest relevant to this article were reported.

Author Contributions. K.M.M. and K.H. designed and coordinated the study, performed most experiments, supervised experiments, analyzed and interpreted data, and wrote the manuscript. D.K., S.V., M.B., L.M., and S.A. provided major technical support. S.J., K.F., T.D.M., and M.H.T. performed metabolic cage experiments and data analyses and interpretation. H.E. assisted in data interpretation and contributed to discussion and experimental design. C.M. performed LC-MS metabolomics and data analyses. J.H. conducted

histopathological liver analyses, assisted in data interpretation, and contributed to discussion and experimental design. T.S. assisted in data interpretation, contributed to discussion and experimental design, and contributed to the writing of the manuscript. N.B. performed LC-MS metabolomics and data analyses, assisted in data interpretation, contributed to discussion and experimental design, and contributed to the writing of the manuscript. J.P.T. and R.M. designed and coordinated the study and wrote the manuscript. J.P.T. and R.M. are the guarantors of this work and, as such, had full access to all the data in the study and take responsibility for the integrity of the data and the accuracy of the data analysis.

References

- Rose AJ, Herzog S. Metabolic control through glucocorticoid hormones: an update. *Mol Cell Endocrinol* 2013;380:65–78
- Geer EB, Islam J, Buettner C. Mechanisms of glucocorticoid-induced insulin resistance: focus on adipose tissue function and lipid metabolism. *Endocrinol Metab Clin North Am* 2014;43:75–102
- Shimizu N, Maruyama T, Yoshikawa N, et al. A muscle-liver-fat signalling axis is essential for central control of adaptive adipose remodelling. *Nat Commun* 2015;6:6693
- Okun JG, Conway S, Schmidt KV, et al. Molecular regulation of urea cycle function by the liver glucocorticoid receptor. *Mol Metab* 2015;4:732–740
- Rosen ED, Spiegelman BM. What we talk about when we talk about fat. *Cell* 2014;156:20–44
- Samuel VT, Shulman GI. The pathogenesis of insulin resistance: integrating signaling pathways and substrate flux. *J Clin Invest* 2016;126:12–22
- Xu C, He J, Jiang H, et al. Direct effect of glucocorticoids on lipolysis in adipocytes. *Mol Endocrinol* 2009;23:1161–1170
- Gray NE, Lam LN, Yang K, Zhou AY, Koliwad S, Wang JC. Angiotensin-like 4 (Angptl4) protein is a physiological mediator of intracellular lipolysis in murine adipocytes. *J Biol Chem* 2012;287:8444–8456
- Yu CY, Mayba O, Lee JV, et al. Genome-wide analysis of glucocorticoid receptor binding regions in adipocytes reveal gene network involved in triglyceride homeostasis. *PLoS One* 2010;5:e15188
- Gathercole LL, Morgan SA, Bujalska IJ, Hauton D, Stewart PM, Tomlinson JW. Regulation of lipogenesis by glucocorticoids and insulin in human adipose tissue. *PLoS One* 2011;6:e26223
- Chimin P, Farias TdaS, Torres-Leal FL, et al. Chronic glucocorticoid treatment enhances lipogenic activity in visceral adipocytes of male Wistar rats. *Acta Physiol (Oxf)* 2014;211:409–420
- Lee MJ, Fried SK, Mundt SS, et al. Depot-specific regulation of the conversion of cortisone to cortisol in human adipose tissue. *Obesity (Silver Spring)* 2008;16:1178–1185
- Engeli S, Böhnke J, Feldpausch M, et al. Regulation of 11β-HSD genes in human adipose tissue: influence of central obesity and weight loss. *Obes Res* 2004;12:9–17
- Masuzaki H, Paterson J, Shinyama H, et al. A transgenic model of visceral obesity and the metabolic syndrome. *Science* 2001;294:2166–2170
- Morton NM, Paterson JM, Masuzaki H, et al. Novel adipose tissue-mediated resistance to diet-induced visceral obesity in 11β-hydroxysteroid dehydrogenase type 1-deficient mice. *Diabetes* 2004;53:931–938
- Kershaw EE, Morton NM, Dhillon H, Ramage L, Seckl JR, Flier JS. Adipocyte-specific glucocorticoid inactivation protects against diet-induced obesity. *Diabetes* 2005;54:1023–1031
- Tronche F, Kellendonk C, Kretz O, et al. Disruption of the glucocorticoid receptor gene in the nervous system results in reduced anxiety. *Nat Genet* 1999; 23:99–103
- Eguchi J, Wang X, Yu S, et al. Transcriptional control of adipose lipid handling by IRF4. *Cell Metab* 2011;13:249–259
- Müller TD, Müller A, Yi CX, et al. The orphan receptor Gpr83 regulates systemic energy metabolism via ghrelin-dependent and ghrelin-independent mechanisms. *Nat Commun* 2013;4:1968

20. Schweiger M, Eichmann TO, Taschler U, Zimmermann R, Zechner R, Lass A. Measurement of lipolysis. *Methods Enzymol* 2014;538:171–193
21. Engblom D, Kornfeld JW, Schwake L, et al. Direct glucocorticoid receptor-Stat5 interaction in hepatocytes controls body size and maturation-related gene expression. *Genes Dev* 2007;21:1157–1162
22. Bajad SU, Lu W, Kimball EH, Yuan J, Peterson C, Rabinowitz JD. Separation and quantitation of water soluble cellular metabolites by hydrophilic interaction chromatography-tandem mass spectrometry. *J Chromatogr A* 2006;1125:76–88
23. Fröhlich EE, Farzi A, Mayerhofer R, et al. Cognitive impairment by antibiotic-induced gut dysbiosis: analysis of gut microbiota-brain communication. *Brain Behav Immun* 2016;56:140–155
24. Yuan M, Breitkopf SB, Yang X, Asara JM. A positive/negative ion-switching, targeted mass spectrometry-based metabolomics platform for bodily fluids, cells, and fresh and fixed tissue. *Nat Protoc* 2012;7:872–881
25. Sumner LW, Amberg A, Barrett D, et al. Proposed minimum reporting standards for chemical analysis Chemical Analysis Working Group (CAWG) Metabolomics Standards Initiative (MSI). *Metabolomics* 2007;3:211–221
26. R Core Team. R: A language and environment for statistical computing. R Foundation for Statistical Computing, Vienna, Austria 2014. Available from <http://www.R-project.org/>. Accessed 2 July 2015
27. Tschöp MH, Speakman JR, Arch JR, et al. A guide to analysis of mouse energy metabolism. *Nat Methods* 2011;9:57–63
28. Wang TJ, Larson MG, Vasan RS, et al. Metabolite profiles and the risk of developing diabetes. *Nat Med* 2011;17:448–453
29. Satapati S, Sunny NE, Kucejova B, et al. Elevated TCA cycle function in the pathology of diet-induced hepatic insulin resistance and fatty liver. *J Lipid Res* 2012;53:1080–1092
30. Rebrin K, Steil GM, Getty L, Bergman RN. Free fatty acid as a link in the regulation of hepatic glucose output by peripheral insulin. *Diabetes* 1995;44:1038–1045
31. Wu Q, Kazantzis M, Doege H, et al. Fatty acid transport protein 1 is required for nonshivering thermogenesis in brown adipose tissue. *Diabetes* 2006;55:3229–3237
32. Badman MK, Pissios P, Kennedy AR, Koukos G, Flier JS, Maratos-Flier E. Hepatic fibroblast growth factor 21 is regulated by PPAR α and is a key mediator of hepatic lipid metabolism in ketotic states. *Cell Metab* 2007;5:426–437
33. Zechner R, Zimmermann R, Eichmann TO, et al. FAT SIGNALS—lipases and lipolysis in lipid metabolism and signaling. *Cell Metab* 2012;15:279–291
34. Li YQ, Shrestha YB, Chen M, Chanturiya T, Gavrilova O, Weinstein LS. Gs α deficiency in adipose tissue improves glucose metabolism and insulin sensitivity without an effect on body weight. *Proc Natl Acad Sci USA* 2016;113:446–451
35. Schreiber R, Hofer P, Taschler U, et al. Hypophagia and metabolic adaptations in mice with defective ATGL-mediated lipolysis cause resistance to HFD-induced obesity. *Proc Natl Acad Sci USA* 2015;112:13850–13855
36. Perry RJ, Zhang XM, Zhang D, et al. Leptin reverses diabetes by suppression of the hypothalamic-pituitary-adrenal axis. *Nat Med* 2014;20:759–763
37. Kumashiro N, Beddow SA, Vatner DF, et al. Targeting pyruvate carboxylase reduces gluconeogenesis and adiposity and improves insulin resistance. *Diabetes* 2013;62:2183–2194
38. Morgan SA, McCabe EL, Gathercole LL, et al. 11 β -HSD1 is the major regulator of the tissue-specific effects of circulating glucocorticoid excess. *Proc Natl Acad Sci USA* 2014;111:E2482–E2491
39. Lacasa D, Agli B, Giudicelli Y. Permissive action of glucocorticoids on catecholamine-induced lipolysis: direct “in vitro” effects on the fat cell beta-adrenoreceptor-coupled-adenylate cyclase system. *Biochem Biophys Res Commun* 1988;153:489–497
40. Bartness TJ, Shrestha YB, Vaughan CH, Schwartz GJ, Song CK. Sensory and sympathetic nervous system control of white adipose tissue lipolysis. *Mol Cell Endocrinol* 2010;318:34–43
41. Scherer T, O’Hare J, Diggs-Andrews K, et al. Brain insulin controls adipose tissue lipolysis and lipogenesis. *Cell Metab* 2011;13:183–194
42. Saito N, Guitart X, Hayward M, Tallman JF, Duman RS, Nestler EJ. Corticosterone differentially regulates the expression of Gs alpha and Gi alpha messenger RNA and protein in rat cerebral cortex. *Proc Natl Acad Sci USA* 1989;86:3906–3910
43. Lim HW, Uhlenhaut NH, Rauch A, et al. Genomic redistribution of GR monomers and dimers mediates transcriptional response to exogenous glucocorticoid in vivo. *Genome Res* 2015;25:836–844
44. Mottillo EP, Balasubramanian P, Lee YH, Weng C, Kershaw EE, Granneman JG. Coupling of lipolysis and de novo lipogenesis in brown, beige, and white adipose tissues during chronic β 3-adrenergic receptor activation. *J Lipid Res* 2014;55:2276–2286
45. Goossens GH. The role of adipose tissue dysfunction in the pathogenesis of obesity-related insulin resistance. *Physiol Behav* 2008;94:206–218
46. Morán-Salvador E, López-Parra M, García-Alonso V, et al. Role for PPAR γ in obesity-induced hepatic steatosis as determined by hepatocyte- and macrophage-specific conditional knockouts. *FASEB J* 2011;25:2538–2550
47. Koonen DP, Jacobs RL, Febbraio M, et al. Increased hepatic CD36 expression contributes to dyslipidemia associated with diet-induced obesity. *Diabetes* 2007;56:2863–2871
48. Wilson CG, Tran JL, Erion DM, Vera NB, Febbraio M, Weiss EJ. Hepatocyte-specific disruption of CD36 attenuates fatty liver and improves insulin sensitivity in HFD-fed mice. *Endocrinology* 2016;157:570–585
49. Wu JW, Wang SP, Casavant S, Moreau A, Yang GS, Mitchell GA. Fasting energy homeostasis in mice with adipose deficiency of desnutrin/adipose triglyceride lipase. *Endocrinology* 2012;153:2198–2207
50. Heckmann BL, Zhang X, Xie X, et al. Defective adipose lipolysis and altered global energy metabolism in mice with adipose overexpression of the lipolytic inhibitor G0/G1 switch gene 2 (GOS2). *J Biol Chem* 2014;289:1905–1916
51. Jaeger D, Schoiswohl G, Hofer P, et al. Fasting-induced G0/G1 switch gene 2 and FGF21 expression in the liver are under regulation of adipose tissue derived fatty acids. *J Hepatol* 2015;63:437–445
52. Liang Q, Zhong L, Zhang J, et al. FGF21 maintains glucose homeostasis by mediating the cross talk between liver and brain during prolonged fasting. *Diabetes* 2014;63:4064–4075
53. Bordag N, Klie S, Jürchott K, et al. Glucocorticoid (dexamethasone)-induced metabolome changes in healthy males suggest prediction of response and side effects. *Sci Rep* 2015;5:15954